9-2020

Biomineralization, Strength and Cytocompatibility Improvement of Bredigite Scaffolds Through Doping/Coating

R. Keihan
K. N. Toosi University of Technology

A. R. Ghorbani
K. N. Toosi University of Technology

E. Salahinejad
K.N.Toosi University of Technology

E. Sharifi
Hamadan University of Medical Sciences

Lobat Tayebi
Marquette University, lobat.tayebi@marquette.edu

Ceramics International, Vol. 46, No. 13 (September 2020): 21056-21063. DOI.

Biomineralization, Strength and Cytocompatibility Improvement of Bredigite Scaffolds Through Doping/Coating

R. Keihan
Faculty of Materials Science and Engineering, K. N. Toosi University of Technology, Tehran, Iran
A.R. Ghorbani
Faculty of Materials Science and Engineering, K. N. Toosi University of Technology, Tehran, Iran
E. Salahinejad
Faculty of Materials Science and Engineering, K. N. Toosi University of Technology, Tehran, Iran
E. Sharifi
Department of Tissue Engineering and Biomaterials, School of Advanced Medical Sciences and Technologies, Hamadan University of Medical Sciences, Hamadan, Iran
L. Tayebi
Marquette University School of Dentistry, Milwaukee, WI, 53233, USA

Abstract

Coprecipitation-derived, sacrificial polymeric (urethane) foam-fabricated bredigite ($Ca_7MgSi_4O_{16}$) scaffolds were processed by individual and combined treatments of fluoride doping and poly (lactic-*co*-glycolic acid) (PLGA) coating and then studied in terms of structure, mechanical strength, bioactivity and cell biocompatibility *in vitro*. According to scanning electron microscopy and Archimedes porosimetry, the geometrical characteristics of pores for all the scaffolds are in the appropriate range for hard tissue regeneration applications. The apatite-formation ability of the samples immersed in a simulated body fluid is improved by doping for both the bare and coated conditions, based on microscopic and energy-dispersive X-ray spectroscopic analyses. Both the treatments advantageously buffer physiological pH changes imposed due to the fast bioresorption of the ceramic. Also, the biodegradable PLGA coating typically enhances the compressive strength of the scaffolds, which is critical for bone tissue engineering. In accordance with the MTT assay on osteoblast-like cells (MG-63) cultures, both the processes individually enhance the cell viability, while the highest improvement is obtained for the combined application of them. It is finally concluded that fluoride doping and PLGA coating are impressive approaches to improve the bioperformance of bredigite-based scaffolds.

Keywords

Silicate (D), Sintering (A), Mechanical properties (C), Biomedical applications (E)

1. Introduction

Among various types of bioresorbable and bioactive ceramics, it is well-known that Ca–Mg silicates have considerable mechanical properties, making them promising for hard tissue engineering applications. In this regard, a relatively wide range of bioresorbability, bioactivity, strength and biocompatibility may be obtained by using this class of bioceramics, including diopside ($CaMgSi_2O_6$) [[1], [2], [3], [4], [5], [6]], akermanite ($Ca_2MgSi_2O_7$) [[7], [8], [9], [10], [11]], merwinite ($Ca_3MgSi_2O_8$) [12,13], monticellite ($CaMgSiO_4$) [14] and bredigite ($Ca_7MgSi_4O_{16}$) [[15], [16], [17]] porous scaffolds. As a result of a high bioresorption rate upon implantation, bredigite disadvantageously increases physiological pH and thereby lacks high biocompatibility [18,19]. Furthermore, as a general drawback, mechanical properties of ceramic scaffolds must be improved for hard tissue engineering applications.

On the one hand, it has been frequently reported that fluoride incorporation at optimal levels into calcium phosphates [20,21], bioactive glasses [[22], [23], [24]], calcium silicate [[25], [26], [27]] and Ca–Mg silicates [[28], [29], [30]] alters their biodegradation, bioactivity and biocompatibility. Typically, fluoride enhances the chemical stability of apatite precipitated during the implantation of bioactive ceramics, thereby increasing their apatite-formation ability. Furthermore, physiological pH is reduced via the exchange of released fluoride ions with the hydroxyl ions of the medium. On the other hand, poly (lactic-*co*-glycolic acid) (PLGA) coating on apatites [[31], [32], [33], [34], [35]], calcium silicate [36,37], bioactive glasses and glass-ceramics [38,39] scaffolds has been shown to modify strength, bioresorbability and biocompatibility. Typically, the biodegradation of PLGA reduces physiological pH via the release of glycolic and lactic acids. Apart from fluoride doping into bredigite particulate bone fillers [40] and the PLGA encapsulation of sol-gel derived bredigite scaffolds [17], there is no report on the combined application of fluoride doping and PLGA coating on tissue-engineering scaffolds to the

best of our knowledge, which are the hypotheses of this work to address the bioperformance of bredigite scaffolds.

2. Experimental procedure

2.1. Preparation of ceramic powders

To synthesize bredigite powders, an inorganic-salt coprecipitation route was used [40]. In brief, calcium chloride ($CaCl_2$, Merck, >98%), magnesium chloride ($MgCl_2$, Merck, >98%) and silicon tetrachloride ($SiCl_4$, Merck, >99%) at the bredigite stoichiometry were dissolved in ethanol (C_2H_5OH, Merck, >99.9%) at 0 °C. Then, ammonia solution (NH_4OH, Merck, 25%) was dropped to pH of almost 10. For fluoride doping at 0.5 mol%, 7% $MgCl_2$ were replaced with the equimolar content of magnesium fluoride (MgF_2, Alfa Aesar, >99%). The achieved precipitates were washed with distilled water, dried at 120 °C and then calcined at 750 °C, at which point they were ready for scaffolding.

2.2. Fabrication of scaffolds

Polyurethane sponges with the open and interconnected porosity of 25 ppi and dimensions of 5×5×5 mm^3 were used as sacrificial scaffolding templates. The foams were treated in 2% sodium hydroxide (NaOH, Merck, Germany, >99%) solution under ultrasonication and then washed with distilled water. The calcined powders were suspended in 7 wt% polyvinyl alcohol aqueous solution at a mass ratio of 1:1 under magnetic stirring and sonication. The foams were then immersed in the slurry to cover all interior and exterior surfaces. In order to blow away the remained slurry and reduce the blockage of pores, the immersed scaffolds were subjected to a compressed airflow. After drying the foams at ambient temperature, they were sintered at 1200 °C. The undoped and fluoride-doped bredigite scaffolds were dipped in 15% wt/v PLGA (LA/GA = 50:50, Corbion, Netherlands)/acetone solution. Then, the coated scaffolds were dried at 60 °C.

2.3. Structural characterization of scaffolds

The morphology of the powders and scaffolds was characterized by a field-emission scanning electron microscope (FESEM, MIRA3TESCAN-XMU, 15 kV). To determine the porosity level of the scaffolds (*P*), the water Archimedes approach with three repetitions was used:

(1)

$$P(\%) = \frac{W_2 - W_1}{W_2 - W_3} \times 100$$

where W_1, W_2, and W_3 are the weight of the dry, wet and immersed scaffolds, respectively.

2.4. Apatite-formation ability of scaffolds

The scaffolds were soaked in the simulated body fluid (SBF) at 36.5 ± 1.5 °C with a solution-to-scaffold ratio of 200 ml g^{-1}. They were afterwards analyzed by FESEM equipped by energy dispersive X-ray spectroscopy (EDS) to compare the apatite-formation ability of the samples. Also, the pH value of the SBF in contact with the scaffolds was measured during incubation every day to the 14th day.

2.5. Mechanical testing of scaffolds

The compressive strength of the scaffolds was measured by a SANTAM STM-1 machine at a crosshead speed of 0.5 mm/min with three repetitions.

2.6. Cytocompatibility of scaffolds

Human osteoblast-like cells (MG-63) were used to evaluate the cytotoxicity of the fabricated scaffolds using the MTT assay. MG-63 cells were cultured in Dulbecco's modified Eagle's medium-low glucose supplemented with 10% fetal bovine serum and 1% penicillin-streptomycin. The scaffolds were sterilized by immersion in 70% alcohol, washing with phosphate-buffered saline and ultraviolet radiation exposure. 10,000 cells were then seeded on the top of each sample in a 24-well plate, followed by the addition of the culture medium and incubation at 37 °C under 5% CO_2 for 24 and 72 h. The culture medium was then removed and 100 µl of dimethyl sulfoxide solution was added for the MTT assay, according to the MTT assay protocol described previously [6]. After 30 min, the optical density of viable cells was measured by a ELISA reader.

3. Results and discussion

Fig. 1 shows the FESEM micrograph of the powders calcined at 750 °C used as the scaffolding feedstocks. The undoped and F-doped powders comprise particles of almost 60 and 140 nm in diameter, respectively. The higher particle size of the F-doped powder is attributed to the fact that fluoride incorporation into silicates generally decreases their melting point [22,29,41,42], hence encouraging the particle coarsening mechanism during calcination.

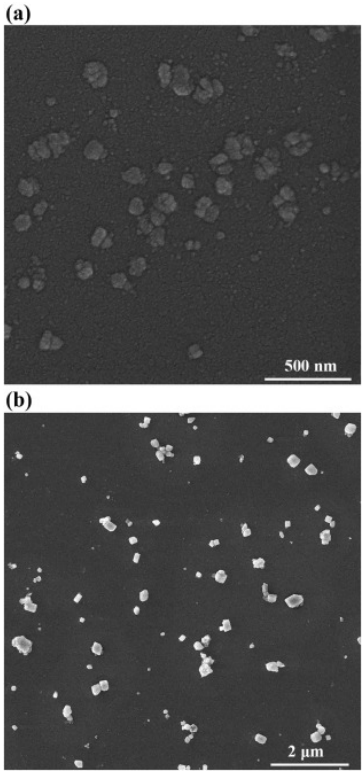

Fig. 1. FESEM micrographs of the undoped (a) and fluoride-doped (b) coprecipitation-derived powders after calcination.

The FESEM micrograph of the scaffolds before immersion in the SBF is represented in Fig. 2. The undoped and F-doped bredigite scaffolds exhibit interconnected porous structures. The mean pore size and struts thickness are about 700 and 120 µm, respectively. After coating with PLGA, a few of the pores are blocked, the mean pore size is reduced, the struts are thickened and the polymer is penetrated into nanopores between the particles. In agreement with the FESEM observations, the porosity level of the bare and coated scaffolds was measured by the water Archimedes porosimetry to be almost 90 and 75%, respectively. Furthermore, the geometrical features of the scaffolds satisfy the bone tissue-engineering requirements ensuring the penetration of cells and nutrients [43,44].

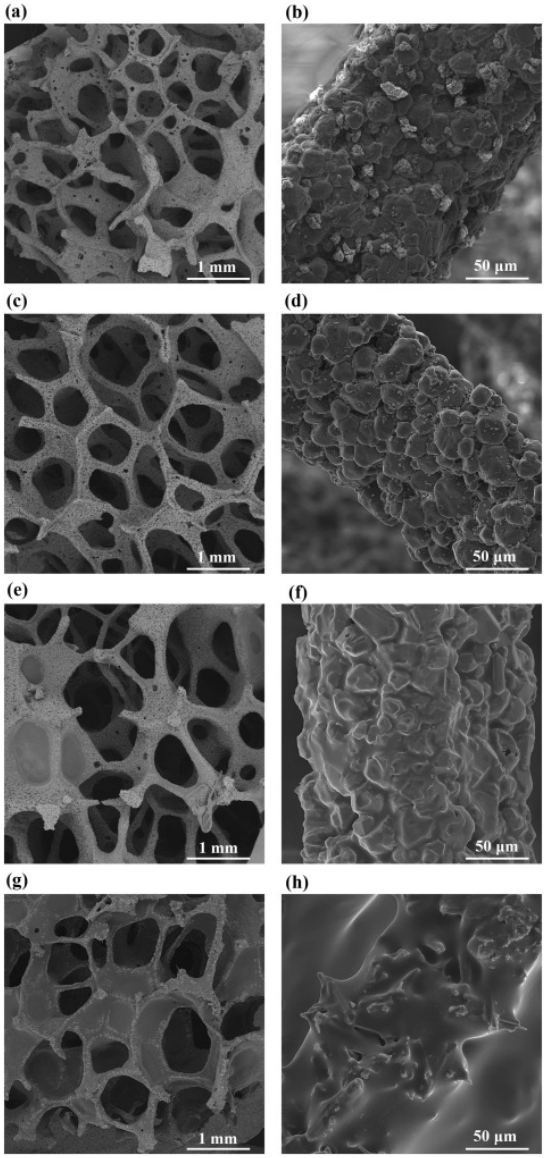

Fig. 2. FESEM micrographs of the undoped (a, b), fluoride-doped (c, d), PLGA-coated undoped (e, f) and PLGA-coated fluoride-doped (g, h) scaffolds after sintering.

Fig. 3 indicates the FESEM micrograph of the scaffolds after incubation in the SBF. As can be observed, the amount of apatite precipitates deposited on the F-doped samples is more than that on the undoped samples for both the bare and coated conditions. This suggests that fluoride doping improves the apatite-formation ability of the bredigite-based scaffolds, as confirmed by the relative intensity of

P, as the main component of apatite, in the EDS profile of the surfaces after immersion in the SBF (Fig. 4). It is also noticeable that the apatite precipitates on the bare samples exhibit a lath-like morphology of 200–500 nm is size, whereas they are changed to worm-like spheres of almost 1 µm in diameter as a result of the PLGA coating.

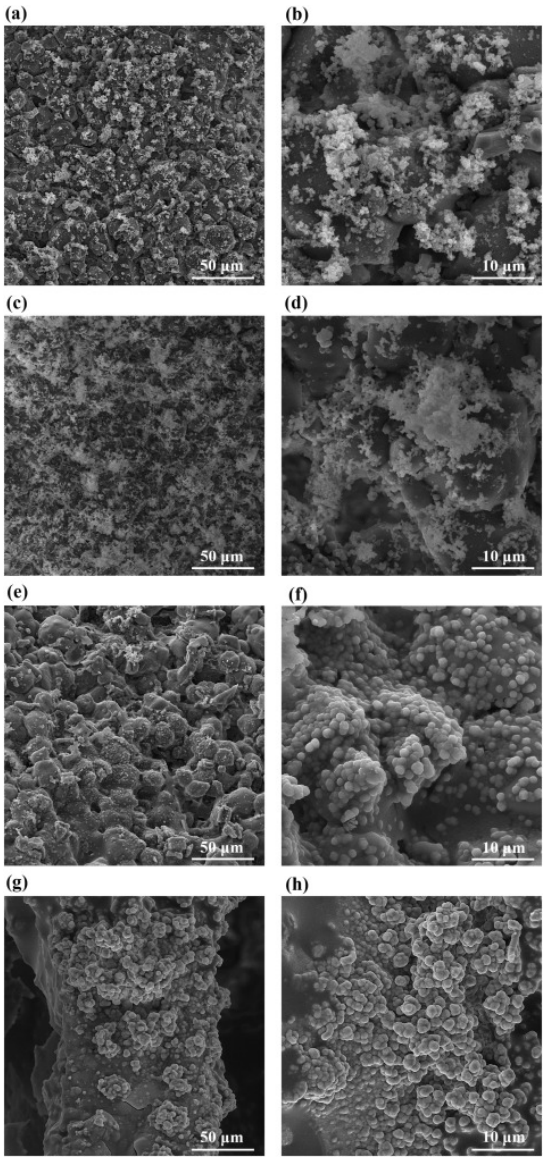

Fig. 3. FESEM micrographs of the undoped (a, b), fluoride-doped (c, d), PLGA-coated undoped (e, f) and PLGA-coated fluoride-doped (g, h) scaffolds after soaking in the SBF.

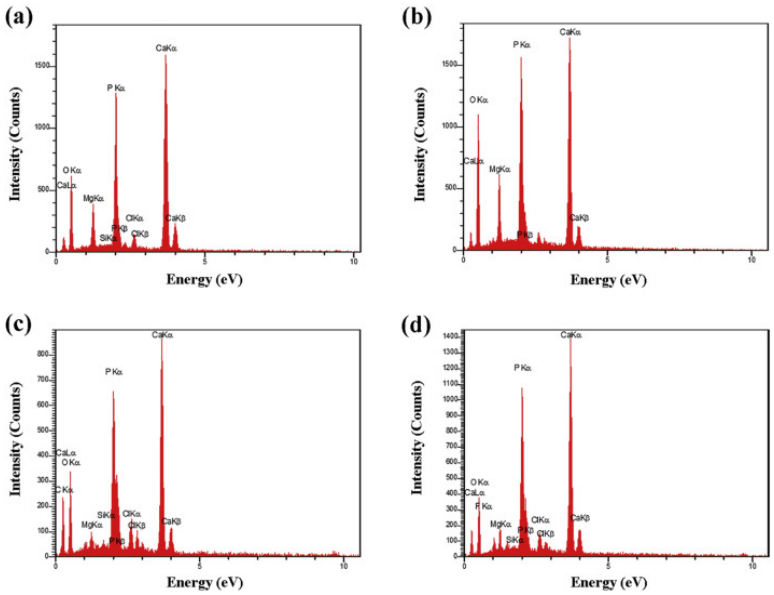

Fig. 4. EDS profiles of the undoped (a), fluoride-doped (b), PLGA-coated undoped (c) and PLGA-coated fluoride-doped (d) scaffolds after soaking in the SBF.

The apatite formation on bredigite is controlled by the ion-exchange mechanism of silicates with the SBF [45,46]. The release of fluoride from the doped samples into the SBF, followed by the incorporation of the suspended fluoride ions into the apatite deposits enhance the chemical stability of apatite against dissolution and thus bioactivity [22,27,47]. However, the dissolution of bredigite and the deposition of the released ions, which are essential for the apatite precipitation and bioactivity, are inhibited by PLGA coating. Additionally, the acidic products of PLGA degradation decrease the pH value of the SBF, encouraging the dissolution of the deposited apatite and decreasing bioactivity [48,49].

Fig. 5 depicts the pH variation of the SBF in contact with the scaffolds. For all the samples, the first sharp enhancement with time is due to the exchange of the bioceramic cations—particularly Ca^{2+}—with H^+ or H_3O^+ of the SBF. After 4th day of exposure, the pH level relatively reaches plateaus due to a balance between the cationic exchange and the apatite formation consuming the OH^- of the SBF. Regarding the comparison of the different samples, for both the bare and coated samples, fluoride doping into bredigite decreases pH due to the exchange of this anion with OH^- of the SBF [22]. In addition, PLGA coating reduces pH more severely than fluoride doping, which can be explained by two mechanisms. First, PLGA limits the dissolution rate of bredigite, the cationic release and the adsorption of H^+ or H_3O^+. Second, the degradation of PLGA releases acidic products into the SBF, buffering physiological pH which is essential for biocompatibility [36,50].

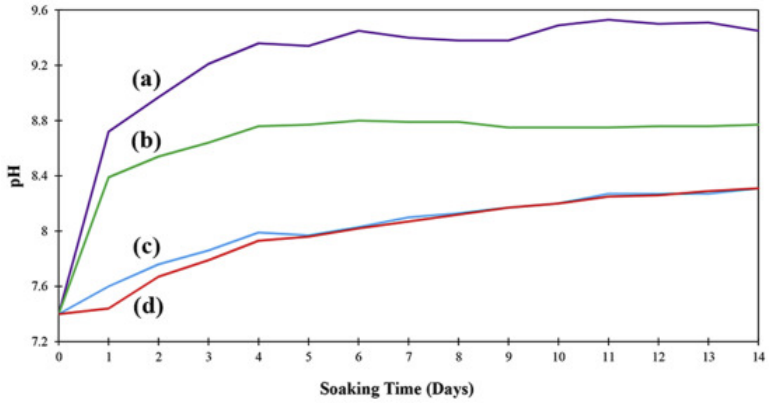

Fig. 5. pH variations of the SBF in contact with the undoped (a), fluoride-doped (b), PLGA-coated undoped (c) and PLGA-coated fluoride-doped (d) scaffolds.

The compressive stress-strain curve of the scaffolds is displayed in Fig. 6. The compressive strength of the bredigite scaffold is around 0.15 MPa. Typically, the strength of the scaffold approaches almost 0.75 MPa after PLGA coating, i.e. an increase of 400%. According to the FESEM micrograph of the samples (Fig. 2) and considering the inherent strength of PLGA, there are three reasons behind this considerable improvement in the compressive strength, including (1) the blockage of some micropores, (2) the penetration of PLGA in the nanopores of the struts and (3) the thickening of the struts because of the PLGA deposition on them. The 15 vol% reduction of the porosity level as a result of PLGA coating, based on the water Archimedes porosimetry, also confirms these contributions to the structural and mechanical variations. It is noticeable that the strength of the PLGA-coated bredigite scaffold fabricated in this work is near that of trabecular bone [[51], [52], [53]] and therefore is suitable for bone tissue engineering.

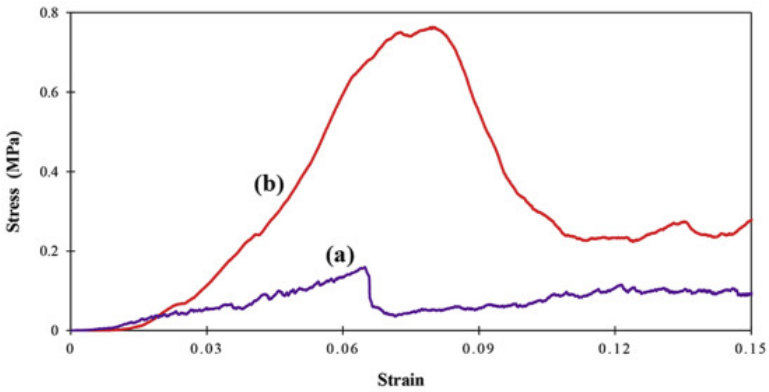

Fig. 6. Compressive stress-strain curve of the bare (a) and PLGA-coated (b) bredigite scaffolds.

The MTT assay results of MG-63 cells cultured on the scaffolds are shown in Fig. 7 with the significance level of $p < 0.05$. The enhancement in the number of viable cells with the culture time is indicative of cell proliferation on the scaffolds. For the first day of cell culture, the cytocompatibility of the undoped bredigite scaffold is lower than the control. However, the other samples do not exhibit a meaningful difference with the respect to the control, showing their considerable biocompatibility. In addition, PLGA coating on both the undoped and doped bredigite scaffolds improves cytocompatibility. For the third day of culture—in contrast to the bare scaffolds—the PLGA-coated samples still preserve their

cytocompatibility near that of the control. Also, fluoride doping and PLGA coating, in both the individual and combined applications, enhance the cytocompatibility of bredigite, where the highest improvement is obtained for the coated and doped scaffold sample. It is also realized that the positive impact of PLGA coating on the cell viability prevails over that of fluoride doping. The cytotoxicity of bredigite is attributed to its high resorption rate, leading to the deteriorous enhancements of physiological pH (Fig. 5) and calcium ions concentration into the medium [54,55]. The buffering effect of fluoride doping and PLGA coating is mostly responsible for the biocompatibility improvement of bredigite. A dose-dependent effect of fluoride on MG-63 cell proliferation has been previously reported [56]. Also, the effect of fluoride doping on the cytocompatibility of bredigite developed in this work is in contrast with that for diopside [6] due to the lower degradation rate and higher biocompatibility of the latter bioceramic.

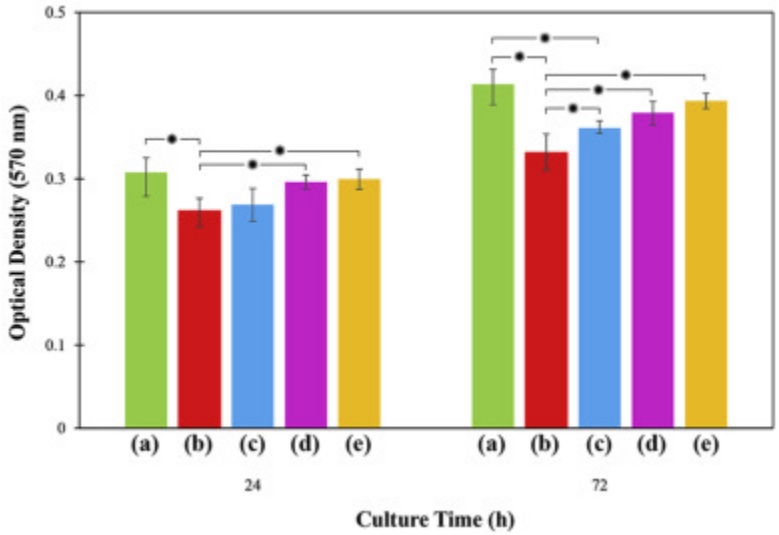

Fig. 7. MTT assay results of MG-63 cells cultured on the control (a), undoped (b), fluoride-doped (c), PLGA-coated undoped (d) and PLGA-coated fluoride-doped (e) scaffolds. * depicts the data having the significant differences ($P < 0.05$).

4. Conclusions

In this work, bredigite porous scaffolds were successfully fabricated by inorganic-salt coprecipitation and foam replica methods. Moreover, fluoride doping into the bredigite structure and PLGA coating on the scaffolds were utilized to improve the biological performance of the scaffolds. The following conclusions can be drawn from this research:

i. Fluoride doping enhanced the apatite-forming ability of the bredigite-based scaffolds, whereas PLGA coating changed the morphology of apatite deposits.
ii. The bredigite scaffold significantly increased the pH value of the SBF when exposed, whereas both fluoride doping and PLGA coating buffered physiological pH.
iii. PLGA coating improved the compressive strength of the bredigite scaffolds by almost 400%.
iv. Fluoride doping and PLGA coating increased the cytocompatibility of bredigite.

Declaration of competing interest

No conflict of interest.

References

[1] C. Wu, Y. Ramaswamy, H. Zreiqat. **Porous diopside (CaMgSi2O6) scaffold: a promising bioactive material for bone tissue engineering.** Acta Biomater., 6 (2010), pp. 2237-2245

[2] H. Ghomi, R. Emadi, S.H. Javanmard. **Fabrication and characterization of nanostructure diopside scaffolds using the space holder method: effect of different space holders and compaction pressures.** Mater. Des., 91 (2016), pp. 193-200

[3] H. Ghomi, R. Emadi, S.H. Javanmard. **Preparation of nanostructure bioactive diopside scaffolds for bone tissue engineering by two near net shape manufacturing techniques.** Mater. Lett., 167 (2016), pp. 157-160

[4] L. Tingting, D. Youwen, G. Chengde, F. Pei, C. Shuai, P. Shuping. **Analysis of 3D printed diopside scaffolds properties for tissue engineering.** Mater. Sci., 21 (2015), pp. 590-594

[5] M. Shahrouzifar, E. Salahinejad. **Strontium doping into diopside tissue engineering scaffolds.** Ceram. Int., 45 (2019), pp. 10176-10181

[6] M. Shahrouzifar, E. Salahinejad, E. Sharifi. **Co-incorporation of strontium and fluorine into diopside scaffolds: bioactivity, biodegradation and cytocompatibility evaluations.** Mater. Sci. Eng. C, 103 (2019), p. 109752

[7] C. Wu, J. Chang, W. Zhai, S. Ni, J. Wang. **Porous akermanite scaffolds for bone tissue engineering: preparation, characterization, and in vitro studies.** J. Biomed. Mater. Res. B, 78 (2006), pp. 47-55

[8] A. Najafinezhad, M. Abdellahi, S. Nasiri-Harchegani, A. Soheily, M. Khezri, H. Ghayour. **On the synthesis of nanostructured akermanite scaffolds via space holder method: the effect of the spacer size on the porosity and mechanical properties.** Journal of the Mechanical Behavior of Biomedical Materials, 69 (2017), pp. 242-248

[9] Z. Han, P. Feng, C. Gao, Y. Shen, C. Shuai, S. Peng. **Microstructure, mechanical properties and in vitro bioactivity of akermanite scaffolds fabricated by laser sintering.** Bio Med. Mater. Eng., 24 (2014), pp. 2073-2080

[10] A. Liu, M. Sun, X. Yang, C. Ma, Y. Liu, X. Yang, S. Yan, Z. Gou. **Three-dimensional printing akermanite porous scaffolds for load-bearing bone defect repair: an investigation of osteogenic capability and mechanical evolution.** J. Biomater. Appl., 31 (2016), pp. 650-660

[11] A. Dasan, H. Elsayed, J. Kraxner, D. Galusek, E. Bernardo. **Hierarchically porous 3D-printed akermanite scaffolds from silicones and engineered fillers.** J. Eur. Ceram. Soc., 39 (2019), pp. 4445-4449

[12] N. Nezafati, M. Hafezi, A. Zamanian, M. Naserirad. **Effect of adding nano-titanium dioxide on the microstructure, mechanical properties and in vitro bioactivity of a freeze cast merwinite scaffold.** Biotechnol. Prog., 31 (2015), pp. 550-556

[13] M. Hafezi, N. Nezafati, A. Nadernezhad, M. Yasaei, A. Zamanian, S. Mobini. **Effect of sintering temperature and cooling rate on the morphology, mechanical behavior and apatite-forming ability of a novel nanostructured magnesium calcium silicate scaffold prepared by a freeze casting method.** J. Mater. Sci., 49 (2014), pp. 1297-1305

[14] H. Bakhsheshi-Rad, X. Chen, A. Ismail, M. Aziz, E. Hamzah, A. Najafinezhad. **A new multifunctional monticellite-ciprofloxacin scaffold: preparation, bioactivity, biocompatibility, and antibacterial properties.** Mater. Chem. Phys., 222 (2019), pp. 118-131

[15] C. Wu, J. Chang, W. Zhai, S. Ni. **A novel bioactive porous bredigite (Ca 7 MgSi 4 O 16) scaffold with biomimetic apatite layer for bone tissue engineering.** J. Mater. Sci. Mater. Med., 18 (2007), pp. 857-864

[16] H. Ghomi, R. Emadi. **Fabrication of bioactive porous bredigite (Ca7MgSi4O16) scaffold via space holder method.** Int. J. Mater. Res., 109 (2018), pp. 257-264

[17] A. Jadidi, E. Salahinejad. **Mechanical strength and biocompatibility of bredigite (Ca7MgSi4O16) tissue-engineering scaffolds modified by aliphatic polyester coatings.** Ceram. Int., 46 (2020), pp. 16439-16446

[18] C. Wu, J. Chang. **Degradation, bioactivity, and cytocompatibility of diopside, akermanite, and bredigite ceramics.** J. Biomed. Mater. Res. B, 83 (2007), pp. 153-160

[19] C. Wu, J. Chang, J. Wang, S. Ni, W. Zhai. **Preparation and characteristics of a calcium magnesium silicate (bredigite) bioactive ceramic.** Biomaterials, 26 (2005), pp. 2925-2931

[20] F. Yao, R.Z. LeGeros. **Carbonate and fluoride incorporation in synthetic apatites: comparative effect on physico-chemical properties and in vitro bioactivity in fetal bovine serum.** Mater. Sci. Eng. C, 30 (2010), pp. 423-430

[21] L. Montazeri, J. Javadpour, M. Shokrgozar, S. Bonakdar, M.K. Moghaddam, V. Asgary. **The interaction of plasma proteins with nano-size fluoride-substituted apatite powders.** Ceram. Int., 39 (2013), pp. 6145-6152

[22] D.S. Brauer, N. Karpukhina, M.D. O'Donnell, R.V. Law, R.G. Hill. **Fluoride-containing bioactive glasses: effect of glass design and structure on degradation, pH and apatite formation in simulated body fluid.** Acta Biomater., 6 (2010), pp. 3275-3282

[23] G. Rajkumar, V. Dhivya, S. Mahalaxmi, K. Rajkumar, G. Sathishkumar, R. Karpagam. **Influence of fluoride for enhancing bioactivity onto phosphate based glasses.** J. Non-Cryst. Solids, 493 (2018), pp. 108-118

[24] F.A. Shah, D.S. Brauer, R.G. Hill, K.A. Hing. **Apatite formation of bioactive glasses is enhanced by low additions of fluoride but delayed in the presence of serum proteins.** Mater. Lett., 153 (2015), pp. 143-147

[25] E. Fuji, K. Kawabata, H. Yoshimatsu, S. Hayakawa, K. Tsuru, A. Osaka. **Structure and biomineralization of calcium silicate glasses containing fluoride ions.** J. Ceram. Soc. Jpn., 111 (2003), pp. 762-766

[26] M. Gandolfi, P. Taddei, F. Siboni, E. Modena, M. Ginebra, C. Prati. **Fluoride-containing nanoporous calcium-silicate MTA cements for endodontics and oral surgery: early fluorapatite formation in a phosphate-containing solution.** Int. Endod. J., 44 (2011), pp. 938-949

[27] P. Taddei, E. Modena, A. Tinti, F. Siboni, C. Prati, M.G. Gandolfi. **Effect of the fluoride content on the bioactivity of calcium silicate-based endodontic cements.** Ceram. Int., 40 (2014), pp. 4095-4107

[28] N. Esmati, T. Khodaei, E. Salahinejad, E. Sharifi. **Fluoride doping into SiO2-MgO-CaO bioactive glass nanoparticles: bioactivity, biodegradation and biocompatibility assessments.** Ceram. Int., 44 (2018), pp. 17506-17513

[29] M.J. Baghjeghaz, E. Salahinejad. **Enhanced sinterability and in vitro bioactivity of diopside through fluoride doping.** Ceram. Int., 43 (2017), pp. 4680-4686
[30] E. Salahinejad, M.J. Baghjeghaz. **Structure, biomineralization and biodegradation of Ca-Mg oxyfluorosilicates synthesized by inorganic salt coprecipitation.** Ceram. Int., 43 (2017), pp. 10299-10306
[31] A. Khojasteh, F. Fahimipour, M.B. Eslaminejad, M. Jafarian, S. Jahangir, F. Bastami, M. Tahriri, A. Karkhaneh, L. Tayebi. **Development of PLGA-coated β-TCP scaffolds containing VEGF for bone tissue engineering.** Mater. Sci. Eng. C, 69 (2016), pp. 780-788
[32] Y. Kang, A. Scully, D.A. Young, S. Kim, H. Tsao, M. Sen, Y. Yang. **Enhanced mechanical performance and biological evaluation of a PLGA coated β-TCP composite scaffold for load-bearing applications.** Eur. Polym. J., 47 (2011), pp. 1569-1577
[33] X. Miao, D.M. Tan, J. Li, Y. Xiao, R. Crawford. **Mechanical and biological properties of hydroxyapatite/tricalcium phosphate scaffolds coated with poly (lactic-co-glycolic acid).** Acta Biomater., 4 (2008), pp. 638-645
[34] X. Miao, L.-P. Tan, L.-S. Tan, X. Huang. **Porous calcium phosphate ceramics modified with PLGA–bioactive glass.** Mater. Sci. Eng. C, 27 (2007), pp. 274-279
[35] X. Huang, X. Miao. **Novel porous hydroxyapatite prepared by combining H2O2 foaming with PU sponge and modified with PLGA and bioactive glass.** J. Biomater. Appl., 21 (2007), pp. 351-374
[36] L. Zhao, K. Lin, M. Zhang, C. Xiong, Y. Bao, X. Pang, J. Chang. **The influences of poly (lactic-co-glycolic acid)(PLGA) coating on the biodegradability, bioactivity, and biocompatibility of calcium silicate bioceramics.** J. Mater. Sci., 46 (2011), pp. 4986-4993
[37] L. Zhao, C. Wu, K. Lin, J. Chang. **The effect of poly (lactic-co-glycolic acid)(PLGA) coating on the mechanical, biodegradable, bioactive properties and drug release of porous calcium silicate scaffolds.** Bio Med. Mater. Eng., 22 (2012), pp. 289-300
[38] R. Björkenheim, G. Strömberg, M. Ainola, P. Uppstu, L. Aalto-Setälä, L. Hupa, J. Pajarinen, N.C. Lindfors. **Bone morphogenic protein expression and bone formation are induced by bioactive glass S53P4 scaffolds in vivo.** J. Biomed. Mater. Res. B, 107 (2019), pp. 847-857
[39] T.M. O'Shea, X. Miao, Preparation and Characterisation of Plga-Coated Porous Bioactive Glass-Ceramic Scaffolds for Subchondral Bone Tissue Engineering, Ceramic Materials and Components for Energy and Environmental Applications, John Wiley & Sons Inc2010, pp. 517-523.
[40] R. Keihan, E. Salahinejad. **Inorganic-salt coprecipitation synthesis, fluoride-doping, bioactivity and physiological pH buffering evaluations of bredigite.** Ceram. Int., 46 (2020), pp. 13292-13296
[41] D.S. Brauer, N. Karpukhina, R.V. Law, R.G. Hill. **Structure of fluoride-containing bioactive glasses.** J. Mater. Chem., 19 (2009), pp. 5629-5636
[42] A. Rafferty, A. Clifford, R. Hill, D. Wood, B. Samuneva, M. Dimitrova-Lukacs. **Influence of fluorine content in apatite–mullite glass-ceramics.** J. Am. Ceram. Soc., 83 (2000), pp. 2833-2838
[43] Q.L. Loh, C. Choong. **Three-dimensional scaffolds for tissue engineering applications: role of porosity and pore size.** Tissue Eng. B Rev., 19 (2013), pp. 485-502
[44] F.J. O'brien. **Biomaterials & scaffolds for tissue engineering.** Mater. Today, 14 (2011), pp. 88-95

[45] S. Ferraris, S. Yamaguchi, N. Barbani, M. Cazzola, C. Cristallini, M. Miola, E. Vernè, S. Spriano. **Bioactive materials: in vitro investigation of different mechanisms of hydroxyapatite precipitation.** Acta Biomater., 102 (2020), pp. 468-480

[46] A.H. Taghvaei, F. Danaeifar, C. Gammer, J. Eckert, S. Khosravimelal, M. Gholipourmalekabadi. **Synthesis and characterization of novel mesoporous strontium-modified bioactive glass nanospheres for bone tissue engineering applications.** Microporous Mesoporous Mater., 294 (2020), p. 109889

[47] Q. Lin, Y. Li, X. Lan, C. Lu, Y. Chen, Z. Xu. **The apatite formation ability of CaF2 doping tricalcium silicates in simulated body fluid.** Biomed. Mater., 4 (2009) 045005

[48] S.H. Rhee, S.J. Lee. **Effect of acidic degradation products of poly (lactic-co-glycolic) acid on the apatite-forming ability of poly (lactic-co-glycolic) acid-siloxane nanohybrid material.** J. Biomed. Mater. Res., 83 (2007), pp. 799-805

[49] I.A. Kim, S.H. Rhee. **Effects of poly (lactic-co-glycolic acid)(PLGA) degradability on the apatite-forming capacity of electrospun PLGA/SiO2–CaO nonwoven composite fabrics.** J. Biomed. Mater. Res. B, 93 (2010), pp. 218-226

[50] C. Wu, Y. Zhang, W. Fan, X. Ke, X. Hu, Y. Zhou, Y. Xiao. **CaSiO3 microstructure modulating the in vitro and in vivo bioactivity of poly (lactide-co-glycolide) microspheres.** J. Biomed. Mater. Res., 98 (2011), pp. 122-131

[51] D.R. Carter, W.C. Hayes. **Bone compressive strength: the influence of density and strain rate.** Science, 194 (1976), pp. 1174-1176

[52] C.E. Misch, Z. Qu, M.W. Bidez. **Mechanical properties of trabecular bone in the human mandible: implications for dental implant treatment planning and surgical placement.** J. Oral Maxillofac. Surg., 57 (1999), pp. 700-706

[53] R. Oftadeh, M. Perez-Viloria, J.C. Villa-Camacho, A. Vaziri, A. Nazarian. **Biomechanics and mechanobiology of trabecular bone: a review.** J. Biomater. Appl. (2015), p. 137

[54] B. Zhivotovsky, S. Orrenius. **Calcium and cell death mechanisms: a perspective from the cell death community.** Cell Calcium, 50 (2011), pp. 211-221

[55] M.V. Peshwa, Y.S. Kyung, D.B. McClure, W.S. Hu. **Cultivation of mammalian cells as aggregates in bioreactors: effect of calcium concentration of spatial distribution of viability.** Biotechnol. Bioeng., 41 (1993), pp. 179-187

[56] Y. Wei, Y. Wu, B. Zeng, H. Zhang. **Effects of sodium fluoride treatment in vitro on cell proliferation, BMP-2 and BMP-3 expression in human osteosarcoma MG-63 cells.** Biol. Trace Elem. Res., 162 (2014), pp. 18-25